

## R-snakes

Lyubomir Zagorchev <sup>a,\*</sup>, Ardeshir Goshtasby <sup>a</sup>, Martin Satter <sup>b</sup>

<sup>a</sup> Department of Computer Science and Engineering, Wright State University, Dayton, OH 45435, USA

<sup>b</sup> Nuclear Medicine/PET, Kettering Medical Center, 3535 Southern Blvd., Kettering, OH 45429, USA

Received 20 May 2005; received in revised form 5 July 2006; accepted 12 July 2006

---

### Abstract

Energy minimizing contours or snakes are tools for delineating objects of interest in an image. Snakes are defined discretely or in continuous form with continuous snakes having advantages over discrete snakes. A continuous snake called B-snake has been previously defined using B-spline curves. In this paper, a continuous snake called R-snake is introduced that is based on rational Gaussian (RaG) curves and has advantages over B-snakes. Not only the stiffness of an R-snake can be varied continuously to delineate an object from coarse to fine, the stiffness of different parts of an R-snake can be adjusted to recover a shape with smooth as well as detailed parts. The formulation of R-snakes is presented and experimental results delineating various objects in synthetic and real images are presented and discussed.

© 2006 Elsevier B.V. All rights reserved.

**Keywords:** Image segmentation; Energy minimizing contours; R-snakes

---

### 1. Introduction and background

An energy minimizing contour or *snake* is a deformable model that conforms to the boundary shape of an object if initialized near the boundary in an image. It can also track an object in an image sequence when initialized at the approximate boundary of the object in one of the frames. A snake continuously deforms to minimize its energy, which is defined by image forces and the snake's internal forces. Because of their ability to approximate complex shapes, snakes have been used in many image analysis applications, including nonrigid motion analysis [1,2] and object tracking [3,4]. Snakes have been used in segmentation of volumetric images also. After segmenting image slices individually, regions obtained in the slices are stacked to form a volumetric region [5–8].

The snake concept was first introduced by Kass et al. [2]. Since its inception, different variations of it have emerged.

Various forces controlling the snake have also been proposed. Forces that drive the snake through spurious features, such as edges, have been proposed by Cohen [7]. Various image features that can decrease the sensitivity of the snake to its initial placement in an image have been explored [9–11] and forces that capture a wide range of shapes and produce boundaries of concave regions have been proposed too [12,13].

Snakes are defined either discretely by a sequence of points [2] or continuously by a parametric curve such as B-Splines [14,15] and nonuniform rational B-Splines (NURBS) [16,17]. In the discrete representation, adjacent snake points are connected to create a continuous boundary. A snake defined by a parametric curve already represents a continuous boundary.

In this paper, a new representation for continuous snakes is described that is based on rational Gaussian (RaG) curves [18]. Snakes defined by RaG curves will be called *R-snakes*. Similar to B-snakes, R-snakes are compact and locally sensitive. Unlike B-snakes, the smoothness of R-snakes can be varied during their evolution, enabling effective delineation of objects from coarse to fine.

\* Corresponding author. Present address: Philips Research North America, Briarcliff Manor, NY 10510, USA. Tel.: +1 914 945 6138.

E-mail address: [Lyubomir.Zagorchev@philips.com](mailto:Lyubomir.Zagorchev@philips.com) (L. Zagorchev).

The remainder of this paper is organized as follows. First, the discrete and continuous snakes are reviewed. Then, the details of R-snakes are provided and experimental results are presented. Finally, properties of R-snakes are explored and concluding remarks are made.

## 2. Discrete snakes

An energy minimizing contour or snake is defined by  $\mathbf{Q}(u) = (x(u), y(u))$ ,  $u \in [0,1]$  with its behavior controlled by its internal and external energies [2],

$$E = \int_0^1 E(\mathbf{Q}(u)) du = \int_0^1 E_{\text{int}}(\mathbf{Q}(u)) + E_{\text{ext}}(\mathbf{Q}(u)) du. \quad (1)$$

Typically, the internal energy of a snake consists of two terms:

$$E_{\text{int}}(\mathbf{Q}(u)) = \frac{1}{2}\alpha(\mathbf{Q}'(u))^2 + \frac{1}{2}\beta(\mathbf{Q}''(u))^2. \quad (2)$$

The first term represents the continuity and the second term represents the stiffness of the snake. In a discrete snake, continuity and stiffness measures are calculated and used only at discrete snake points. The spacing between adjacent points is used to quantify the snake's continuity. By minimizing this term, snake points are made to have uniform spacing. Without this term, many snake points may converge to the same image point. The angle between adjacent line segments obtained by connecting three consecutive snake points quantify the stiffness of the snake. By maximizing this angle, a snake is made smoother. Without this term, the snake may produce sharp corners and fluctuations.  $\alpha$  and  $\beta$  are two weights defining the contributions of continuity and stiffness on the snake.

The forces that move the snake points towards the image features define the external energy. Depending on the type of image features used, different external energies may be obtained. An external energy that moves the snake points towards image edges is defined by

$$E_{\text{ext}}(\mathbf{Q}(u)) = -|\nabla G(s) * I(\mathbf{Q}(u))|^2, \quad (3)$$

where  $I(\mathbf{Q}(u))$  denotes intensities at and surrounding the snake point at parameter  $u$ ,  $G$  is a two-dimensional Gaussian of standard deviation  $s$  pixels,  $*$  denotes convolution, and  $\nabla$  is a gradient operator.

By substituting (2) into (1), we obtain

$$E = \int_0^1 \frac{1}{2}\alpha(\mathbf{Q}'(u))^2 + \frac{1}{2}\beta(\mathbf{Q}''(u))^2 + E_{\text{ext}}(\mathbf{Q}(u)) du. \quad (4)$$

Letting  $y = \mathbf{Q}(u)$ ,  $y' = \mathbf{Q}'(u)$ , and  $y'' = \mathbf{Q}''(u)$ , the total energy of a snake can be represented by the general formula

$$E = \int_0^1 F(u, y, y', y'') du. \quad (5)$$

From the calculus of variations [19], the minimum of (5) is found to be a function  $y(u)$  that produces a minimum. If  $\bar{y}(u) = y(u) + \varepsilon\eta(u)$  is the set of admissible functions, where

$y(u)$  is the function of interest,  $\varepsilon$  is a numerical parameter, and  $\eta(u)$  is a twice differentiable function for which

$$\eta(0) = \eta(1) = \eta'(0) = \eta'(1) = 0, \quad (6)$$

then, we can write

$$\bar{y}'(u) = y'(u) + \varepsilon\eta'(u), \quad (7)$$

$$\bar{y}''(u) = y''(u) + \varepsilon\eta''(u). \quad (8)$$

After substituting  $\bar{y}, \bar{y}', \bar{y}''$  into (5) we obtain

$$E = \int_0^1 F(u, y + \varepsilon\eta, y' + \varepsilon\eta', y'' + \varepsilon\eta'') du. \quad (9)$$

Since  $y(u)$  produces a minimum for  $E$ , the integral must have a minimum for  $\varepsilon = 0$ , so that its derivative can vanish. This implies:

$$\frac{dE}{d\varepsilon} = \int_0^1 \left( \frac{\partial F}{\partial y} \eta + \frac{\partial F}{\partial y'} \eta' + \frac{\partial F}{\partial y''} \eta'' \right) du = 0. \quad (10)$$

Using integration by parts and the endpoint conditions for  $\eta'$ , the third term in (10) can be expressed by

$$\begin{aligned} \int_0^1 \frac{\partial F}{\partial y''} \eta'' du &= \left[ \frac{\partial F}{\partial y''} \eta' \right]_0^1 - \int_0^1 \eta' \frac{d}{du} \left( \frac{\partial F}{\partial y''} \right) du \\ &= - \int_0^1 \eta' \frac{d}{du} \left( \frac{\partial F}{\partial y''} \right) du. \end{aligned} \quad (11)$$

Integrating by parts again, but now using the endpoint conditions for  $\eta$ , we have

$$\begin{aligned} \int_0^1 \frac{\partial F}{\partial y''} \eta'' du &= - \left[ \eta \frac{d}{du} \left( \frac{\partial F}{\partial y''} \right) \right]_0^1 + \int_0^1 \eta \frac{d^2}{du^2} \left( \frac{\partial F}{\partial y''} \right) du = \\ &= \int_0^1 \eta \frac{d^2}{du^2} \left( \frac{\partial F}{\partial y''} \right) du. \end{aligned} \quad (12)$$

Using integration by parts and the same endpoint conditions, the second term can be re-written as

$$\int_0^1 \frac{\partial F}{\partial y'} \eta' du = - \int_0^1 \eta \frac{d}{du} \left( \frac{\partial F}{\partial y'} \right) du. \quad (13)$$

Putting these together, we obtain

$$\frac{dE}{d\varepsilon} = \int_0^1 \left( \frac{\partial F}{\partial y} - \frac{d}{du} \left( \frac{\partial F}{\partial y'} \right) + \frac{d^2}{du^2} \left( \frac{\partial F}{\partial y''} \right) \right) \eta du = 0. \quad (14)$$

If this is true for an arbitrary function  $\eta(u)$ , then the following, also known as the Euler–Lagrange equation, must be true

$$\frac{\partial F}{\partial y} - \frac{d}{du} \left( \frac{\partial F}{\partial y'} \right) + \frac{d^2}{du^2} \left( \frac{\partial F}{\partial y''} \right) = 0. \quad (15)$$

Going back to the original equation, we have

$$\frac{\partial F}{\partial y} = \nabla E_{\text{ext}}(\mathbf{Q}(u)), \quad (16)$$

$$\frac{d}{du} \left( \frac{\partial F}{\partial y'} \right) = \alpha \frac{d}{du} \mathbf{Q}'(u) = \alpha \mathbf{Q}''(u), \quad (17)$$

$$\frac{d^2}{du^2} \left( \frac{\partial F}{\partial y} \right) = \beta \frac{d^2}{du^2} \mathbf{Q}''(u) = \beta \mathbf{Q}'''(u). \quad (18)$$

Substituting (16), (17), and (18) into (15), we obtain

$$-\alpha \mathbf{Q}''(u) + \beta \mathbf{Q}'''(u) + \nabla E_{\text{ext}}(\mathbf{Q}(u)) = 0. \quad (19)$$

After discretizing Eq. (19), decoupling it with respect to both spatial parameters,  $x$  and  $y$ , estimating the derivatives by finite differences, and letting  $\mathbf{F} = \nabla E_{\text{ext}}(\mathbf{Q}(u))$ , we obtain

$$\begin{aligned} & \alpha_i(x_i - x_{i-1}) - \alpha_{i+1}(x_{i+1} - x_i) + \beta_{i-1}(x_{i-2} - 2x_{i-1} + x_i) \\ & - 2\beta_i(x_{i-1} - 2x_i + x_{i+1}) + \beta_{i+1}(x_i - 2x_{i+1} + x_{i+2}) \\ & + Fx_i \\ & = 0, \end{aligned} \quad (20)$$

$$\begin{aligned} & \alpha_i(y_i - y_{i-1}) - \alpha_{i+1}(y_{i+1} - y_i) + \beta_{i-1}(y_{i-2} - 2y_{i-1} + y_i) \\ & - 2\beta_i(y_{i-1} - 2y_i + y_{i+1}) + \beta_{i+1}(y_i - 2y_{i+1} + y_{i+2}) \\ & + Fy_i \\ & = 0, \end{aligned} \quad (21)$$

where  $\mathbf{F} = (Fx, Fy)$ . In matrix form, these equations may be written as

$$\mathbf{Ax} + \mathbf{F}_x = 0, \quad (22)$$

$$\mathbf{Ay} + \mathbf{F}_y = 0, \quad (23)$$

where  $\mathbf{A}$  is a pentadiagonal matrix of coefficients depending on terms  $\alpha$  and  $\beta$ , and  $\mathbf{F}_x$  and  $\mathbf{F}_y$  are vectors representing values for  $Fx$  and  $Fy$  at the snake points. The solution of Eqs. (22) and (23) is found by making them dynamic in time:

$$\mathbf{Ax}_{t+1} + \mathbf{F}_x = -\gamma(\mathbf{x}_{t+1} - \mathbf{x}_t), \quad (24)$$

$$\mathbf{Ay}_{t+1} + \mathbf{F}_y = -\gamma(\mathbf{y}_{t+1} - \mathbf{y}_t), \quad (25)$$

where  $\gamma$  is the step size in time. The internal forces in Eqs. (24) and (25) are evaluated at time  $t+1$  rather than  $t$  because the banded matrix is completely defined by the constant coefficients. At equilibrium, the following solution is obtained:

$$\mathbf{x}_{t+1} = (\mathbf{A} + \gamma \mathbf{I})^{-1}(\gamma \mathbf{x}_t - \mathbf{F}_x), \quad (26)$$

$$\mathbf{y}_{t+1} = (\mathbf{A} + \gamma \mathbf{I})^{-1}(\gamma \mathbf{y}_t - \mathbf{F}_y). \quad (27)$$

When converged,  $\mathbf{x}_{t+1}$  and  $\mathbf{y}_{t+1}$  will show arrays representing the  $x$  and  $y$  coordinates of the snake points.

### 3. B-Snakes

B-spline snakes or *B-snakes* are widely used tools in image segmentation [15,14]. B-snakes have been used in the reconstruction of 3-D organs by delineating and stacking the segmented regions in image slices [20]. A 3-D representation is obtained by tracking the regions delimited by the evolution of a snake in a sequence of slices. A framework for the interactive segmentation of ultrasound images using B-snakes has been proposed [21]. The segmentation is performed slice by slice. Due to the low quality of

ultrasound images, the operator is allowed to correct inaccuracies in segmentation. Multiple B-snakes have been applied simultaneously to segment a complex object [22]. A snake is used to represent a segment of the object and all snakes are smoothly joined according to a blending scheme. Wang et al. [23] proposed using a structure-adaptive B-snake to segment complex objects. The snake is initialized using a small number of control points. More control points are then added during its evolution until the object is well localized. Variations of this algorithm have been used to delineate objects in medical images [24] and track objects in videos [25].

A B-snake is defined by a B-Spline curve [14], which consists of curve segments smoothly joining. Each curve segment represents a polynomial of a given degree. The polynomial is defined as a linear combination of B-spline blending functions  $\{B_i(u): i = 0, \dots, n\}$  and uses control points  $\{\mathbf{V}_i = (X_i, Y_i): i = 0, \dots, n\}$  as the coefficients:

$$\mathbf{Q}(u) = \sum_{i=0}^n \mathbf{V}_i B_i(u) = \sum_{i=0}^n [X_i B_i(u), Y_i B_i(u)]. \quad (28)$$

The total energy of a B-snake is obtained by substituting  $\mathbf{Q}(u)$  in Eq. (1) with the equation of a B-spline curve. That is,

$$\begin{aligned} E = & \sum_{j=0}^m \left\{ \alpha \left[ \left( \sum_{i=0}^n X_i B'_i(u_j) \right)^2 + \left( \sum_{i=0}^n Y_i B'_i(u_j) \right)^2 \right] \right. \\ & + \beta \left[ \left( \sum_{i=0}^n X_i B''_i(u_j) \right)^2 + \left( \sum_{i=0}^n Y_i B''_i(u_j) \right)^2 \right] \\ & \left. + E_{\text{ext}} \left[ \sum_{i=0}^n (X_i B_i(u_j), Y_i B_i(u_j)) \right] \right\}. \end{aligned} \quad (29)$$

The control points that minimize the above total energy must satisfy:

$$\begin{cases} \frac{\partial E}{\partial X_i} = 0, \\ \frac{\partial E}{\partial Y_i} = 0, \end{cases} \quad \forall i \in \{0, \dots, n\}. \quad (30)$$

After finding the partial derivatives of the total energy with respect to the control point coordinates, setting them to zero, and following the procedure outlined for discrete snakes, we obtain:

$$\mathbf{A}_b \mathbf{x} + \mathbf{F}_x = 0, \quad (31)$$

$$\mathbf{A}_b \mathbf{y} + \mathbf{F}_y = 0, \quad (32)$$

where  $\mathbf{A}_b$  again is a pentadiagonal matrix of coefficients. To solve Eqs. (31) and (32), they are made dynamic and solved to obtain

$$\mathbf{x}_{t+1} = (\mathbf{A}_b + \gamma \mathbf{I})^{-1}(\gamma \mathbf{x}_t - \mathbf{F}_x), \quad (33)$$

$$\mathbf{y}_{t+1} = (\mathbf{A}_b + \gamma \mathbf{I})^{-1}(\gamma \mathbf{y}_t - \mathbf{F}_y). \quad (34)$$

This process is described in more detail in [14].

In some implementation of B-snakes [26,23–25], the internal energy of the snake is not explicitly used because

the B-spline itself has an implicit internal energy. The snake is moved towards image features only by the influence of the external forces. This is equivalent to setting matrix  $\mathbf{A}_b$  in Eqs. (33) and (34) to zero. If desired, an explicit internal energy may be defined in Eqs. (33) and (34) to further characterize the behavior of the snake [14].

## 4. R-Snakes

### 4.1. RaG curves

Rational Gaussian or RaG curves have been proposed by Goshtasby [18]. A RaG curve with control points  $\{\mathbf{V}_i = (X_i, Y_i): i = 0, \dots, n\}$  is defined by

$$\mathbf{Q}(u) = \sum_{i=0}^n \mathbf{V}_i g_i(u) \quad u \in [0, 1], \quad (35)$$

where

$$g_i(u) = \frac{W_i G_i(u)}{\sum_{j=0}^n W_j G_j(u)} \quad (36)$$

is the  $i$ th blending function of the curve,  $W_i$  is the weight of the  $i$ th control point, and

$$G_i(u) = \exp \left\{ -(u - u_i)^2 / 2\sigma_i^2 \right\} \quad (37)$$

is a Gaussian of height 1 and standard deviation  $\sigma_i$  centered at  $u_i$ .  $\{u_i: i = 0, \dots, n\}$  are known as the nodes of the curve. Node  $u_i$  is the parameter value at which the influence of control point  $\mathbf{V}_i$  is maximum on the curve. The nodes of a curve are set proportional to the cumulative chord length from  $\mathbf{V}_i$  to  $\mathbf{V}_0$ . The standard deviations and the nodes of a RaG curve are measured with the same unit.

The weight of a control point shows the degree of influence of that control point on the curve. The larger the weight, the more the curve is pulled towards that control point. A control point with a weight of 0 will have no influence on the generated curve, while a negative weight will push the curve away from the control point.

Unlike a B-spline curve that uses fixed blending functions, RaG blending functions can be varied by changing the standard deviations of Gaussians along the curve.

The standard deviation of a Gaussian defines the degree of local influence of the associating control point on the curve. A larger standard deviation allows a control point to have a wider influence on the curve, while a smaller standard deviation makes the influence of a control point more local. As a result, as the standard deviations of Gaussians are decreased, the obtained RaG curve will follow its control points more closely and reproduce more details in data. As the standard deviations of Gaussians are increased, the curve smoothes local details in data, generating a smoother boundary. This is shown in Fig. 1. In this example, the same standard deviation was used for all Gaussians in a curve.

Closed RaG curves can be obtained by replacing Eq. (37) with

$$G_i(u) = \sum_{j=-\infty}^{\infty} \exp \left\{ -[u - (u_i - j)]^2 / 2\sigma_i^2 \right\}. \quad (38)$$

The infinity comes from the fact that a Gaussian extends from  $-\infty$  to  $\infty$ , and when the curve is closed, it makes infinite cycles around it. However, since Gaussians approach 0 exponentially, it is only necessary to vary  $j$  from  $-\lceil \sigma(-2 \ln \epsilon)^{1/2} \rceil$  to  $\lceil \sigma(-2 \ln \epsilon)^{1/2} \rceil$  when the standard deviation of all Gaussians is  $\sigma$  and  $\epsilon$  is the accuracy of the computation [18]. Fig. 2 shows three closed RaG curves with the same control points, weights, and nodes, but different standard deviations. In this example also, the same standard deviation was used for all Gaussians in a curve.

### 4.2. Contour initialization

An R-snake can be initialized in an image either by: (1) selecting the control points of the snake interactively, or (2) estimating its control points by fitting a RaG curve to a sequence of image points with a required tolerance. In the first case, the RaG curve will be obtained immediately because the control points are known. In the second case, the control points are determined by solving a system of linear equations by the least-squares method.

Given a sequence of image points  $\{\mathbf{P}_k: k = 0, \dots, N\}$ , the set of control points  $\{\mathbf{V}_i: i = 0, \dots, n\}$  of the RaG curve approximating the image points can be determined by minimizing

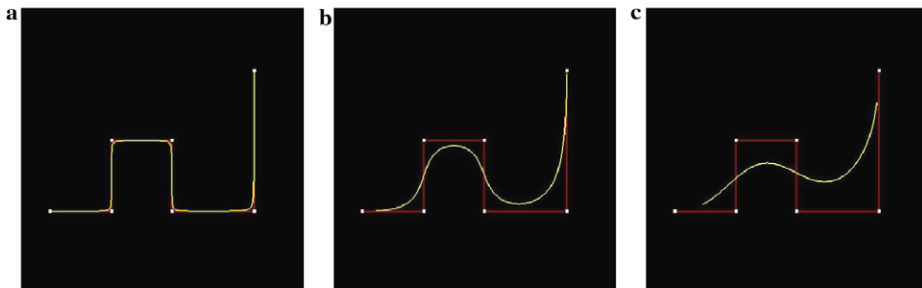


Fig. 1. (a)–(c) Three RaG curves with different standard deviations approximating the same set of control points. Standard deviations in (a)–(c) are 0.05, 0.1, and 0.15, respectively.

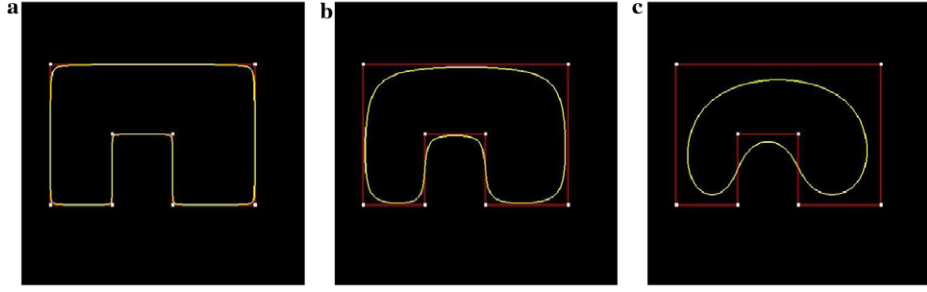


Fig. 2. (a)–(c) Three closed RaG curves with different standard deviations approximating the same set of control points. Standard deviations in (a)–(c) are 0.045, 0.06, and 0.085, respectively.

$$E_2 = \sum_{k=0}^N \left\| \mathbf{P}_k - \frac{\sum_{i=0}^n \mathbf{V}_i W_i \exp\{-(u_k - u_i)^2 / 2\sigma^2\}}{\sum_{j=0}^n W_j \exp\{-(u_k - u_j)^2 / 2\sigma^2\}} \right\|^2, \quad (39)$$

where  $N > n$ . To minimize (39), partial derivatives of  $E_2$  with respect to  $\{\mathbf{V}_i : i = 0, \dots, n\}$  are determined, the derivatives are set to zero, and the obtained system of equations is solved for the control points. Since control point  $\mathbf{V}_i$  has two components  $(X_i, Y_i)$ , relation (39) is actually written in terms of its  $X$  and  $Y$  components and the partial derivatives are determined with respect to  $X_i$  and  $Y_i$  for  $i = 0, \dots, n$ . The system of equations obtained for each component is then solved to obtain the  $X$  and  $Y$  components of the control points independently.

When  $N = n$ ,  $E_2 = 0$  and the coordinates of the control points are obtained by solving two systems of linear equations in  $X_i$  and  $Y_i$  for  $i = 0, \dots, n$  directly and without the least-squares.

Due to the monotonically decreasing nature of RaG blending functions, the obtained matrix of coefficients will be diagonally dominant. As the standard deviations of Gaussians are decreased, the diagonal elements become more distinct and as the standard deviations of Gaussians are increased, the off-diagonal elements become more similar to the diagonal elements, causing the system of equations to become ill-conditioned. Since arbitrarily small standard deviations can be used, the system of equations can always be solved. To simplify the computations and to allow control of an entire curve with a single parameter, the standard deviations of all Gaussians are set to a common parameter  $\sigma$ . The common standard deviation is then determined to ensure that the matrix of coefficients has a condition number below a predefined value [18]. In addition, the number of control points ( $n + 1$ ) can be determined so that  $E_2 < \varepsilon$ , where  $\varepsilon$  is the error tolerance in curve fitting.

#### 4.3. Energy formulation

Given an R-snake defined by  $\mathbf{Q}(u) = (X(u), Y(u))$ , where  $u \in [0, 1]$ , its total energy is defined by

$$E = \int_0^1 \frac{1}{2}\alpha(\mathbf{Q}'(u))^2 + \frac{1}{2}\beta(\mathbf{Q}''(u))^2 + E_{\text{ext}}(\mathbf{Q}(u)) du. \quad (40)$$

From the calculus of variations [19], again, the minimum energy of (40) is found from the solution of the following Euler–Lagrange equation:

$$-\alpha\mathbf{Q}''(u) + \beta\mathbf{Q}'''(u) + \nabla E_{\text{ext}}(\mathbf{Q}(u)) = 0. \quad (41)$$

Letting the gradient of the external force at curve point  $\mathbf{Q}(u)$  be

$$\nabla E_{\text{ext}}(\mathbf{Q}(u)) = (F_x(u), F_y(u)), \quad (42)$$

by substituting (42) into (41), discretizing, and decoupling the obtained result with respect to both spatial parameters  $x$  and  $y$ , the following two equations are obtained

$$-\alpha_i X_i'' + \beta_i X_i''' + Fx_i = 0, \quad (43)$$

$$-\alpha_i Y_i'' + \beta_i Y_i''' + Fy_i = 0, \quad (44)$$

where  $\{\mathbf{V}_i = (X_i, Y_i) : i = 0, \dots, n\}$  are the control points of the RaG curve,  $\alpha_i$  and  $\beta_i$  are the contributions of continuity and smoothness at each node, and  $Fx_i$  and  $Fy_i$  are the first derivatives of the external force at  $\mathbf{V}_i$  with respect to the spatial parameters  $x$  and  $y$ .

To determine the external forces and their gradients  $(F_x, F_y)$  at the control points, external forces of curve points at nodes corresponding to the control points are used. This is necessary because the energy at the snake points rather than at the control points should be minimized. Therefore, letting

$$f_x(u_j) = \kappa \sum_{i=0}^M g_i(u_j) Fx_i, \quad (45)$$

$$f_y(u_j) = \kappa \sum_{i=0}^M g_i(u_j) Fy_i, \quad (46)$$

where  $\kappa$  is a scaling factor that controls the degree of influence of the external forces on the snake and  $g_i(u)$  is the RaG blending function associated with  $\mathbf{V}_i$ , we have

$$(f_x(u_j), f_y(u_j)) = \nabla E_{\text{ext}}(\mathbf{Q}(u_j)). \quad (47)$$

Fig. 3 depicts interpretation of Eq. (46). The rational Gaussian blending function  $g_i$ , centered at node  $u_i$ , shows the influence of the  $Y$ -component gradient at control point  $\mathbf{V}_i$  on the curve. As the standard deviation of the Gaussian decreases, the R-snake will approach the nearby image feature more closely. Increasing the standard deviation causes the control point to more globally influence the curve. The

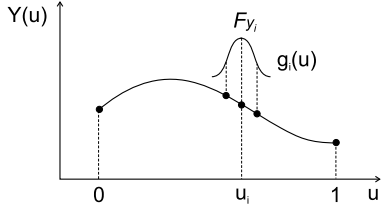


Fig. 3. Influence of image gradients surrounding the curve point at node  $u_i$  on the curve.

standard deviations of Gaussians define the smoothness/detailedness of the obtained curve and the local stiffness/elasticity of the snake. The larger the value for  $\sigma_i$ , the smoother the curve will be at and surrounding the  $i$ th node. If local information about the shape to be recovered is not known, standard deviations of all Gaussians should be set to a common parameter  $\sigma$ . This enables controlling the stiffness of the entire snake by varying a single parameter.

In R-snakes also we will use

$$E_{\text{ext}}(\mathbf{Q}(u)) = -|\nabla G(s) * I(\mathbf{Q}(u))|^2 \quad (48)$$

as the external energy. Other external energies have been used to control continuous snakes before [12,13].

#### 4.4. Iterative minimization

Knowing a set of control points  $\{\mathbf{V}_i = (X_i, Y_i); i = 0, \dots, n\}$  and computing the derivatives by the finite differences method, Eqs. (43) and (44) can be written as

$$\begin{aligned} \alpha_i(X_i - X_{i-1}) - \alpha_{i+1}(X_{i+1} - X_i) + \beta_{i-1}(X_{i-2} - 2X_{i-1} \\ + X_i) - 2\beta_i(X_{i-1} - 2X_i + X_{i+1}) + \beta_{i+1}(X_i - 2X_{i+1} \\ + X_{i+2}) + Fx_i = 0, \end{aligned} \quad (49)$$

$$\begin{aligned} \alpha_i(Y_i - Y_{i-1}) - \alpha_{i+1}(Y_{i+1} - Y_i) + \beta_{i-1}(Y_{i-2} - 2Y_{i-1} \\ + Y_i) - 2\beta_i(Y_{i-1} - 2Y_i + Y_{i+1}) + \beta_{i+1}(Y_i - 2Y_{i+1} \\ + Y_{i+2}) + Fy_i = 0. \end{aligned} \quad (50)$$

Letting

$$\begin{aligned} a &= \beta_{i-1}, \\ b &= -\alpha_i - 2\beta_{i-1} - 2\beta_i, \\ c &= \alpha_{i+1} + \beta_{i+1} + 4\beta_i + \beta_{i+1}, \\ d &= -\alpha_{i+1} - 2\beta_i - 2\beta_{i+1}, \\ e &= \beta_{i+1}, \end{aligned}$$

relations (43) and (44) in matrix form become

$$\mathbf{A}_r \mathbf{X} + \mathbf{F}_x = 0, \quad (51)$$

$$\mathbf{A}_r \mathbf{Y} + \mathbf{F}_y = 0, \quad (52)$$

where  $\mathbf{X}$ ,  $\mathbf{Y}$  are vectors representing the  $X$  and  $Y$  coordinates of the control points,  $\mathbf{F}_x$  and  $\mathbf{F}_y$  are vectors representing the components of the gradients used as the external forces at the control points, and  $\mathbf{A}_r$  is an  $(n+1) \times (n+1)$  matrix of coefficients in terms of  $a$ ,  $b$ ,  $c$ ,  $d$ , and  $e$ . If the snake represents an open curve,  $\mathbf{A}_r$  is the pentadiagonal matrix shown in Fig. 4a, and if the snake is closed, the set of control points has to be made circular to introduce values in the lower-left and upper-right corners of  $\mathbf{A}_r$ , as shown in Fig. 4b.

Note that the above equations are the same as those for the discrete snakes, but the points now represent the control points of the RaG curve. A snake represented by a parametric curve requires a smaller number of control points than the number of points used in a discrete snake to represent a shape.

To find the solution of Eqs. (51) and (52), as described in Section (2), they are solved iteratively as a function of time:

$$\mathbf{X}_{t+1} = (\mathbf{A}_r + \gamma \mathbf{I})^{-1}(\gamma \mathbf{X}_t - \mathbf{F}_x), \quad (53)$$

$$\mathbf{Y}_{t+1} = (\mathbf{A}_r + \gamma \mathbf{I})^{-1}(\gamma \mathbf{Y}_t - \mathbf{F}_y). \quad (54)$$

When the process converges, the coordinates of the control points of an R-snake will be obtained approximating locally maximum gradients along a region in an image.

## 5. Results

In this section, the ability of R-snakes in shape recovery is illustrated. In a set of experiments, a number of shapes

| <b>a</b> | c   | d | e | 0 | 0 | 0 | 0 | 0 | ... | 0 |
|----------|-----|---|---|---|---|---|---|---|-----|---|
| b        | c   | d | e | 0 | 0 | 0 | 0 | 0 | ... | 0 |
| a        | b   | c | d | e | 0 | 0 | 0 | 0 | ... | 0 |
| 0        | a   | b | c | d | e | 0 | 0 | 0 | ... | 0 |
| 0        | 0   | a | b | c | d | e | 0 | 0 | ... | 0 |
| .        | .   | . | . | . | . | . | . | . | ... | . |
| 0        | ... | 0 | 0 | a | b | c | d | e | 0   | 0 |
| 0        | ... | 0 | 0 | 0 | a | b | c | d | e   | 0 |
| 0        | ... | 0 | 0 | 0 | 0 | a | b | c | d   | e |
| 0        | ... | 0 | 0 | 0 | 0 | 0 | a | b | c   | d |

| <b>b</b> | c | d   | e | 0 | 0 | 0 | 0 | 0 | ... | a | b |
|----------|---|-----|---|---|---|---|---|---|-----|---|---|
| b        | c | d   | e | 0 | 0 | 0 | 0 | 0 | ... | 0 | a |
| a        | b | c   | d | e | 0 | 0 | 0 | 0 | ... | 0 | 0 |
| 0        | a | b   | c | d | e | 0 | 0 | 0 | ... | 0 | 0 |
| 0        | 0 | a   | b | c | d | e | 0 | 0 | ... | 0 | 0 |
| .        | . | .   | . | . | . | . | . | . | ... | . | . |
| 0        | 0 | ... | 0 | a | b | c | d | e | 0   | 0 | 0 |
| 0        | 0 | ... | 0 | 0 | a | b | c | d | e   | 0 | 0 |
| 0        | 0 | ... | 0 | 0 | 0 | a | b | c | d   | e | 0 |
| e        | 0 | ... | 0 | 0 | 0 | a | b | c | d   | 0 | 0 |
| d        | e | ... | 0 | 0 | 0 | 0 | a | b | c   | 0 | 0 |

Fig. 4. Matrix  $\mathbf{A}_r$  for (a) an open R-snake and (b) a closed R-snake.

were synthetically generated with a graphics editor. An R-snake was initialized in each image and the energy of the snake was minimized iteratively as described above until the snake converged to the shape. The top left images in Figs. 5–8 show the shapes to be recovered. The top middle images show the initial positions of the R-snakes in the images. Next, the three intermediate results depicting movement of the snakes towards the shapes are shown. The final results are depicted in the bottom right. As can be observed, R-snakes can recover from very smooth shapes to shapes containing very sharp corners. In these experiments, image gradient magnitude was used to calculate the external energy. The images were first smoothed

with a Gaussian filter of standard deviation one pixel before finding the gradient magnitudes. In each experiment, the stiffness parameter  $\sigma$  was kept unchanged during the iterations. Later we will see how to gradually increase the number of control points of an R-snake as its stiffness parameter is reduced to delineate a boundary from coarse to fine.

In another set of experiments, an R-snake was first used to segment an object of interest in an image. Then, the obtained snake was used to track the object boundary in subsequent image slices in a volumetric image. The top left image in Fig. 9 shows an axial CT slice. Initialization of an R-snake near the right kidney is shown in the top middle

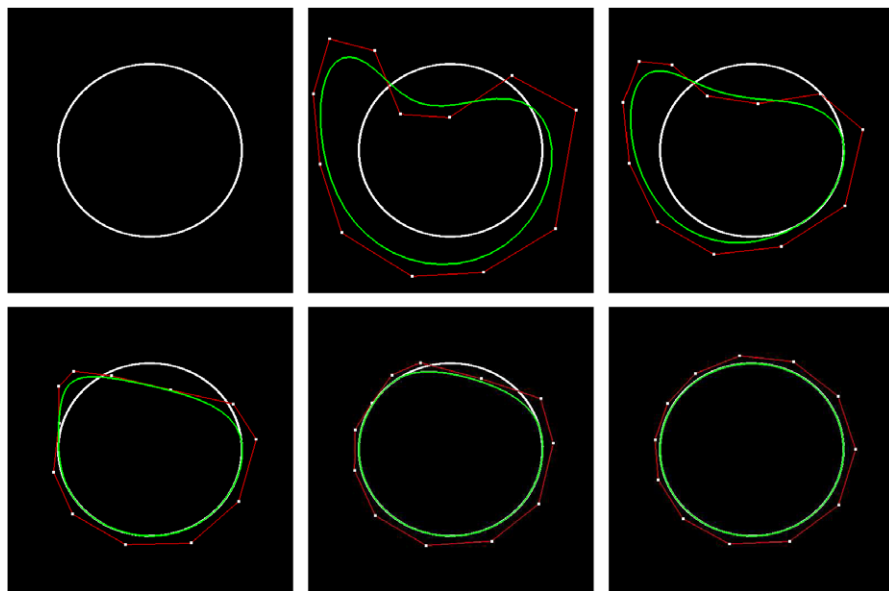


Fig. 5. An R-snake finding a circle.

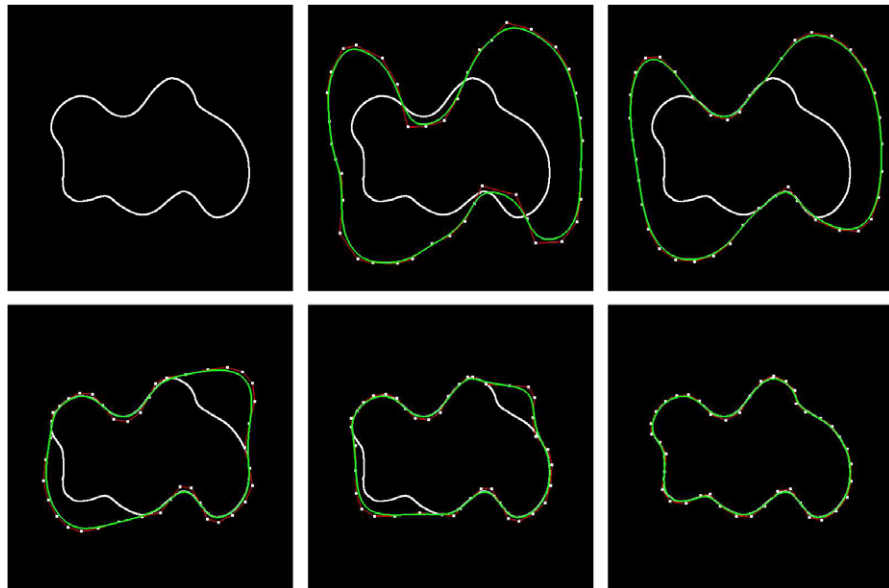


Fig. 6. An R-snake finding a blob.

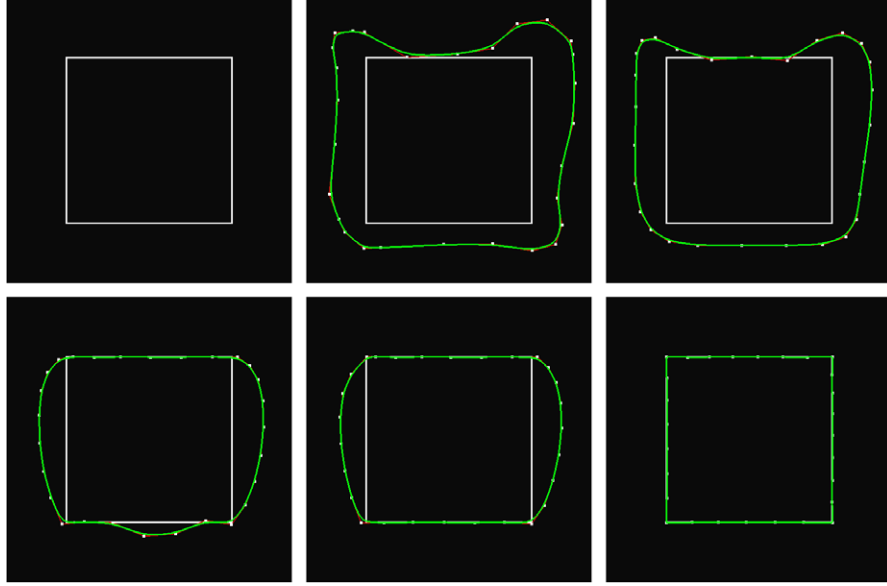


Fig. 7. An R-snake finding a square.

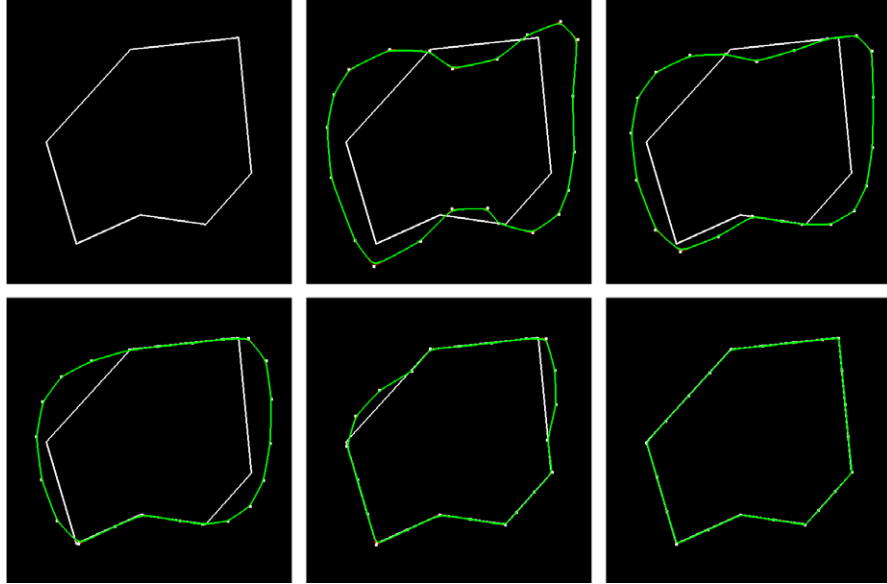


Fig. 8. An R-snake finding a polygon.

image. Three intermediate results showing the evolution of the snake towards the boundary of the kidney are shown next. The final segmentation result is shown in the bottom right. The boundary of the segmented kidney in Fig. 9 was then used to track the cross-sections of the kidney in subsequent slices as depicted in Fig. 10. Again, gradient magnitude was used to calculate the external energy.

In the next experiment, the axial MR brain slice shown in the top-left image in Fig. 11 was used. The top-left image shows an R-snake initialized near the boundary of the resected tumor. Four intermediate results showing the evolution of the snake towards the boundary of the tumor are shown next. The final segmentation result is shown in the

bottom-right. Using the obtained result as the initial position of an R-snake in the next image slice, the subsequent images were segmented, as shown in Fig. 12.

Finally, the axial MR brain slice shown by the top-left image in Fig. 13 was used. Here the objective is to delineate the ventricular boundary. Initialization of an R-snake in the slice near the ventricular boundary is shown in the top-middle image. Similar to previous examples, three intermediate results and the final result are shown. Using the segmentation result obtained in Fig. 13 in a number of subsequent slices, the results shown in Fig. 14 were obtained. The standard deviation of the Gaussian smoother in Figs. 9–14 was one pixel. In these images, a rather small

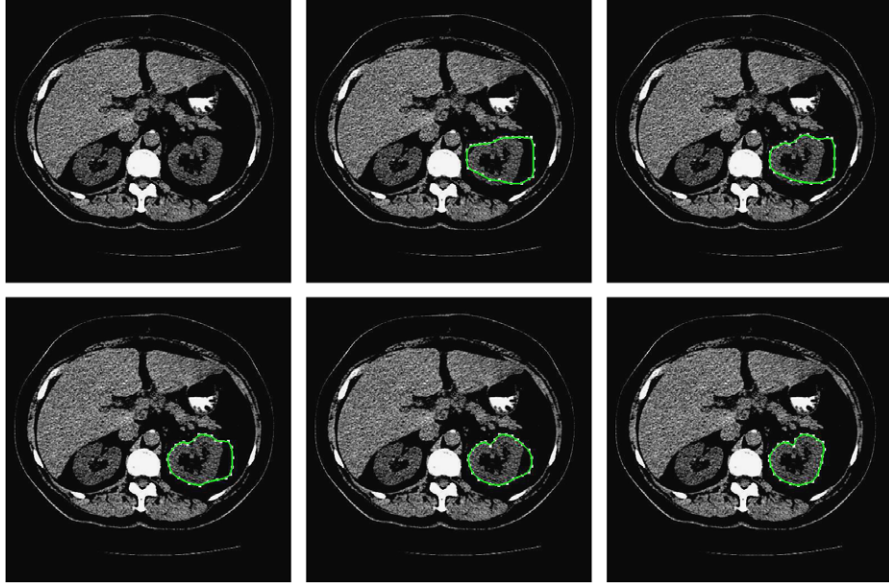


Fig. 9. Delineation of the right kidney in an axial CT slice by an R-snake.

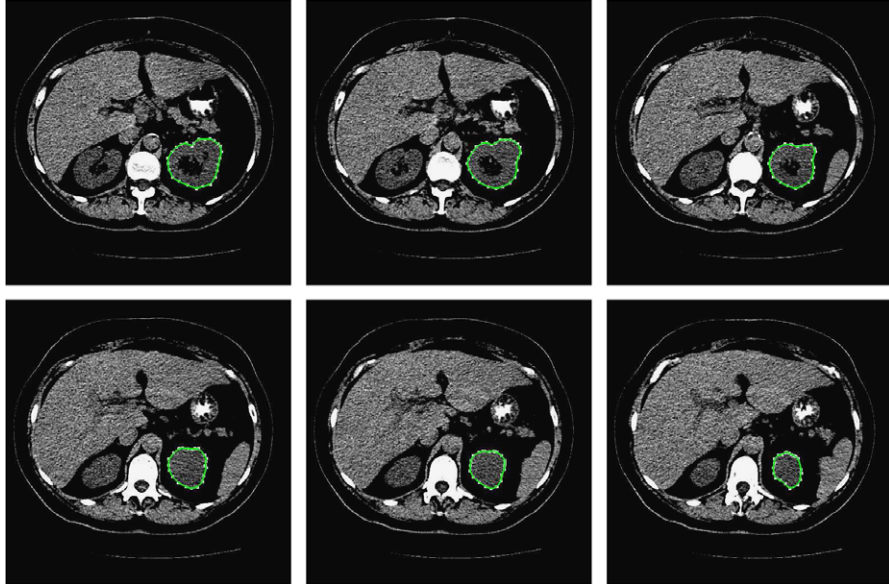


Fig. 10. Tracking the boundary of the right kidney in consecutive axial slices by an R-snake.

stiffness parameter was used to retrieve fine shape details. In Figs. 9–14, the same stiffness parameter was used with external energy computed using gradient magnitudes.

The parameters of the R-snakes used in the experiments are summarized in Tables 1 and 2. Parameters  $\alpha$ ,  $\beta$ , and  $\kappa$  were kept fixed in all the experiments. A wide range of parameters  $\alpha$ ,  $\beta$ , and  $\kappa$  actually work in the above experiments. The stiffness of an R-snake is controlled by parameter  $\sigma$ . The larger the stiffness, the smoother the obtained curve will be. As  $\sigma$  is reduced, the snake becomes more elastic, reproducing more image details. In the experiments using synthetic images, parameter  $\sigma$  was set proportional to the smoothness of the shapes to be recovered. Shapes with sharp corners were given smaller  $\sigma$ s than smoother shapes. In

experiments involving real images, parameter  $\sigma$  was given a rather small value to make the snakes closely follow the boundary details. As we will see later, to achieve a coarse-to-fine segmentation, parameter  $\sigma$  can be initially set to a large value and its value can be gradually decreased as a larger number of control points is used to describe the shape being recovered in more detail. Parameter  $\gamma$  determines the correction step size in each iteration of the snake. The smaller this parameter, the larger the motion of the snake will be. The number of iterations needed for a snake to converge depends on the number of control points used to represent the snake and the distance of the initial snake position to its final position. In the following section, properties of snakes with varying stiffness parameters are explored.

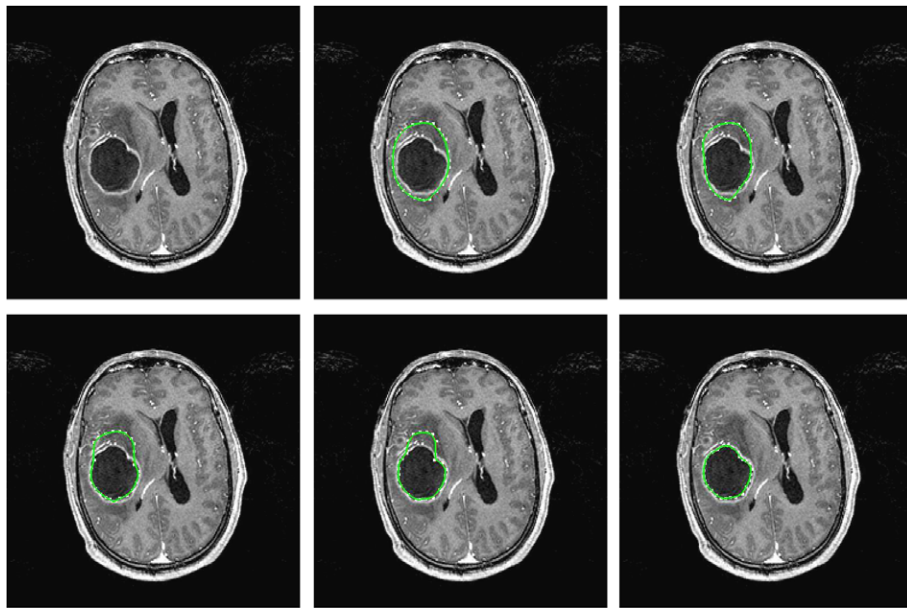


Fig. 11. Delineation of a resected tumor in an axial MR brain slice.

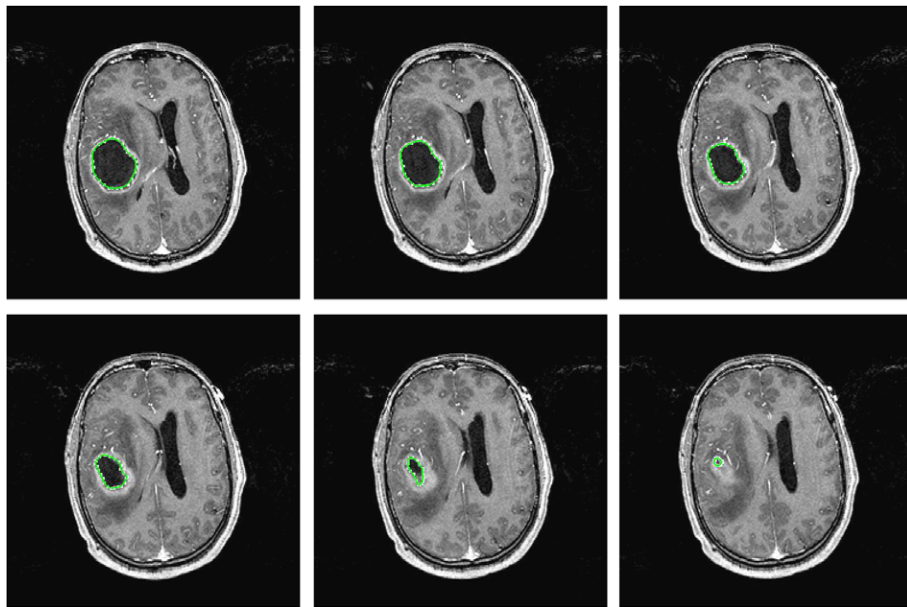


Fig. 12. Tracking the tumor boundary in a sequence of MR brain slices by an R-snake.

## 6. Role of the stiffness parameter

Compared to discrete snakes, continuous snakes have a number of advantages. Since in a continuous snake a smooth curve is used to define a boundary, with a given error tolerance, a smaller number of control points is needed to represent the boundary compared to a discrete snake. Curve-based snakes produce continuous and smooth boundaries that can be displayed at an arbitrary resolution. B-Spline and NURBS curves have been used to define continuous snakes in the past. The main difference between a B-snake and an R-snake is that the B-snake has a fixed

stiffness throughout its evolution, while the stiffness of the R-snake changes throughout its evolution to localize itself more accurately in an image.

### 6.1. Dependence of stiffness on accuracy

To determine the influence of the stiffness parameter  $\sigma$  of an R-Snake on the recovered shapes, a number of experiments were carried out using synthetic and real images. In each experiment, the R-snake was initialized at the same set of control points but parameter  $\sigma$  was changed. For each point in the converged R-snake, the closest point on the

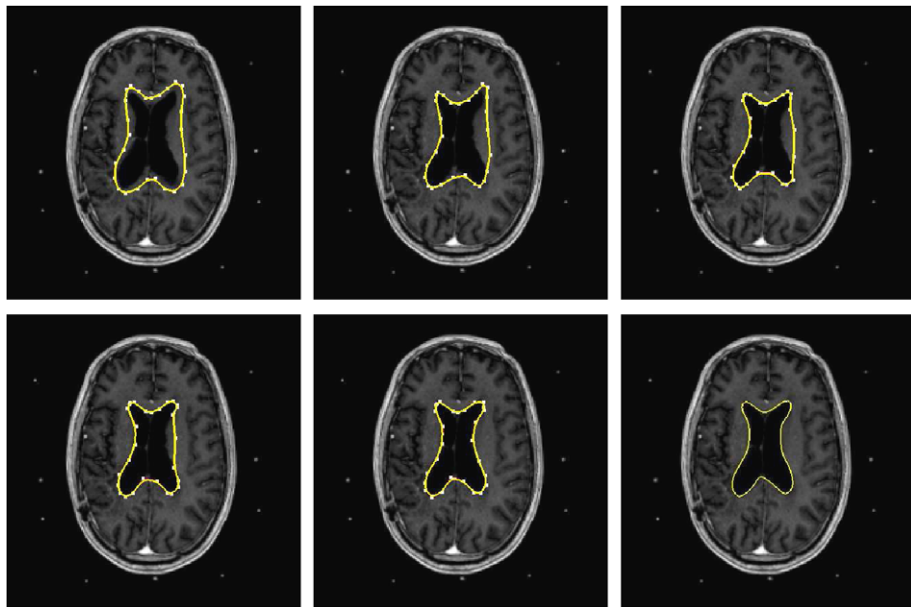


Fig. 13. Delineation of the brain ventricles in an axial MR brain slice.

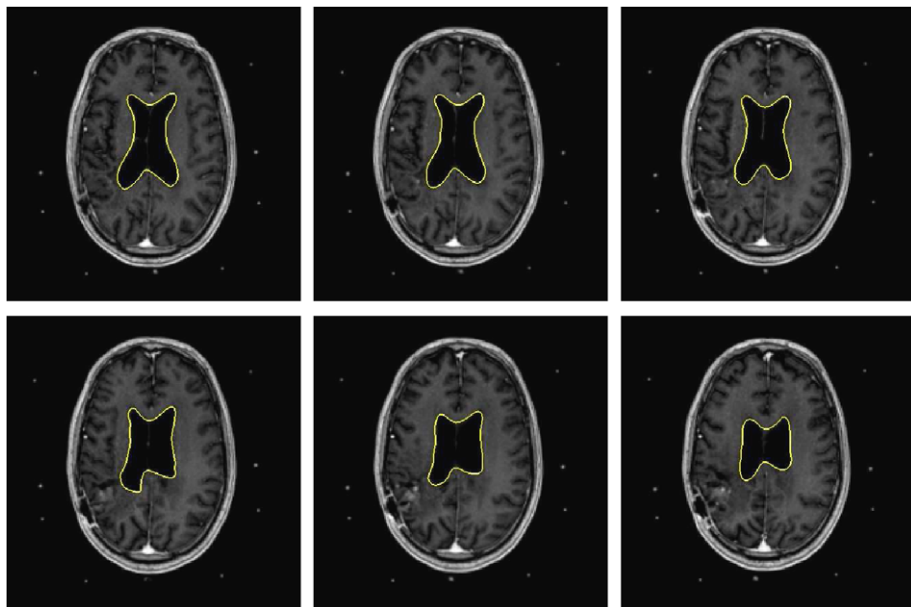


Fig. 14. Tracking the ventricular boundary in a sequence of axial MR slices by an R-snake.

**Table 1**  
Parameters of the R-snakes used in synthetic images

| Image   | Control points | $\sigma$ | $\alpha$ | $\beta$ | $\gamma$ | $\kappa$ |
|---------|----------------|----------|----------|---------|----------|----------|
| Circle  | 12             | 0.070    | 0.002    | 0.000   | 1        | 2        |
| Blob    | 42             | 0.030    | 0.002    | 0.000   | 1        | 2        |
| Square  | 28             | 0.015    | 0.002    | 0.000   | 1        | 2        |
| Polygon | 22             | 0.015    | 0.002    | 0.000   | 1        | 2        |

**Table 2**  
Parameters of the R-snakes in real images

| Image     | Control points | $\sigma$ | $\alpha$ | $\beta$ | $\gamma$ | $\kappa$ | No. iterations |
|-----------|----------------|----------|----------|---------|----------|----------|----------------|
| Body      | 26             | 0.015    | 0.002    | 0.000   | 1        | 2        | 509            |
| Brain     | 27             | 0.015    | 0.002    | 0.000   | 1        | 2        | 478            |
| Ventricle | 28             | 0.015    | 0.002    | 0.000   | 1        | 2        | 413            |

shape to be recovered was determined and the root-mean-squared (RMS) error and the maximum (MAX) error were computed and tabulated. In experiments using synthetic

images, points on the shapes were used. In experiments using real images, the edge points in the images were detected and errors were calculated between points in the snake and the closest edge points.

Figs. 15 and 16 contain a circle and a triangle, respectively. These shapes were recovered by R-snakes using the same initial control points but different stiffnesses. Figs. 15(c)–(h) and 16(c)–(h) show recovered shapes with standard deviations equal to 0.015, 0.025, 0.035, 0.045, 0.055, and 0.065, respectively. When the standard deviations are very small, the snake approximating a circle approaches a discrete snake and approximates the circle by a polygon. This indicates that when a very elastic snake is used to approximate a very smooth shape, the number of control points of the snake should be proportionately increased to enable better localization of the snake. Knowing the nature of the shape to be recovered, the standard deviation of the Gaussians and, thus, the number of control points of the snake can be selected. If the nature of the shape to be recovered is not known, one should start with a rather stiff snake and gradually reduce its stiffness depending on the image gradients at the nodes of the curve. If image gradi-

ents at some nodes are very small, it could be an indication that the stiffness of the curve is too high. In such a situation, the stiffness of the snake should be decreased and the control points should be proportionately increased to enable the snake to bend easily and localize itself more accurately in an image.

In Fig. 16, as the stiffness parameter is increased, the error increases. In order to reproduce sharp corners in a shape, there is a need to use a more elastic snake. As the stiffness of the snake is reduced, its control points should be increased to reproduce the local details. Knowing that parameter  $u$  of a snake varies from 0 to 1 and parameters  $u$  and  $\sigma$  are measured with the same unit, once  $\sigma$  is chosen, we let  $n = 1/2\sigma$ . This will cause the snake point at a node to be influenced more than 80% by the corresponding control point than by other control points. Using a larger number of control points will be a waste; however, if we use a smaller number of control points

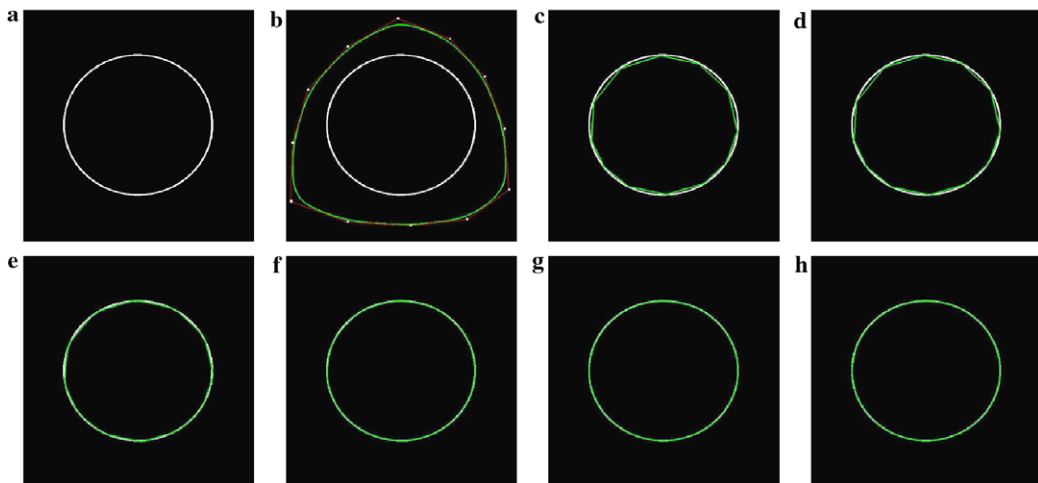


Fig. 15. Detecting a circle. (a) The circle. (b) The initialized R-snake. (c)–(h) Results with standard deviations 0.015, 0.025, 0.035, 0.045, 0.055, and 0.065, respectively.

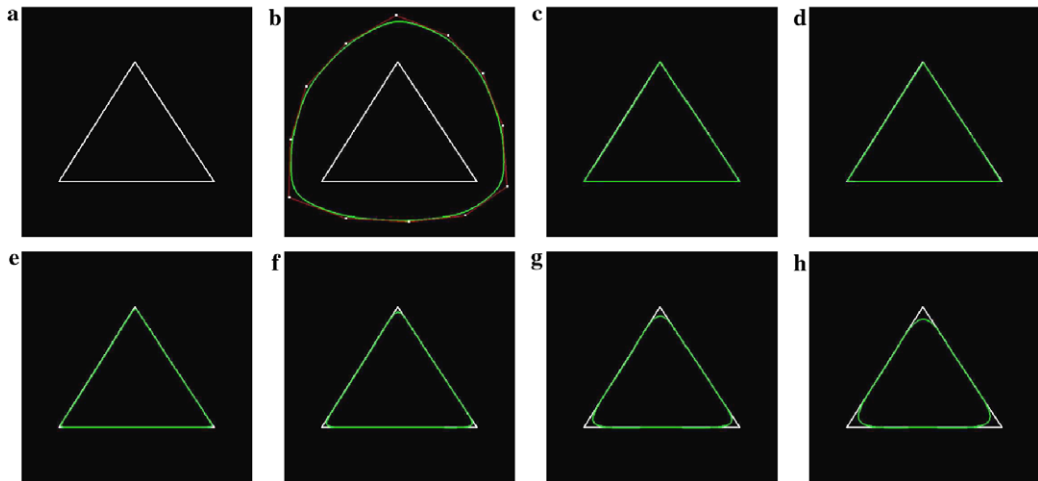


Fig. 16. Detecting a triangle. (a) The triangle. (b) The initial snake. (c)–(h) The detection results using the R-snakes with the same initial control points and stiffness parameters 0.015, 0.025, 0.035, 0.045, 0.055, and 0.065, respectively.

we may not have a sufficient number of control points to reproduce local shape details for a particular stiffness parameter. In a snake where stiffness is defined locally, the stiffness of the snake at the node where the gradient is low is reduced to half its value and instead two new control points are inserted at its sides to allow the snake to locally bend and reproduce local shape details better. In a homogeneous area, if two new control points are inserted and the gradient at the node does not increase, this indicates that the newly added control points are not improving the situation and can be eliminated. This will avoid wasteful control points in segments of a snake that lie in homogeneous image areas.

Fig. 17 shows segmentation of the brain ventricles in an axial MR brain slice. The edges of the axial slice that were used to calculate the RMS and MAX errors are shown in Fig. 17(b). The segmentation results using R-snakes with

stiffness parameters 0.015, 0.025, 0.035, 0.045, 0.055, and 0.065 are shown in Fig. 17(c)–(h), respectively.

Fig. 18 shows delineation of a resected brain tumor in an axial MR brain slice. The axial slice is shown in Fig. 18(a). The edges of the axial slice that were used to calculate the RMS and MAX errors are shown in Fig. 18(b). The segmentation results using R-snakes with the initial control points shown in Fig. 11 and standard deviations 0.015, 0.025, 0.035, 0.045, 0.055, and 0.065 are shown in Fig. 18(c)–(h), respectively.

The RMS and MAX segmentation errors of the synthetic and real images are shown in Fig. 19. For the same number of control points, as the stiffness parameter is increased, RMS and MAX errors decrease when a very smooth shape like a circle is being recovered. For shapes containing detailed segments, increasing the stiffness parameter increases the errors as expected.

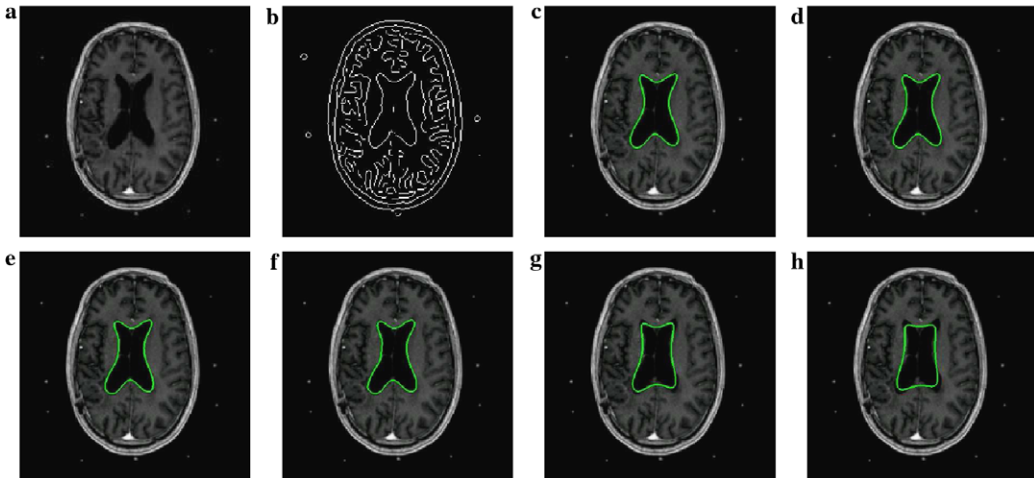


Fig. 17. Delineating the brain ventricles in an axial MR brain slice. (a) The axial slice. (b) The edges of the axial slice. (c)–(h) The segmentation results using R-snakes with the initial control points shown in Fig. 13 and stiffness parameters 0.015, 0.025, 0.035, 0.045, 0.055, and 0.065, respectively.

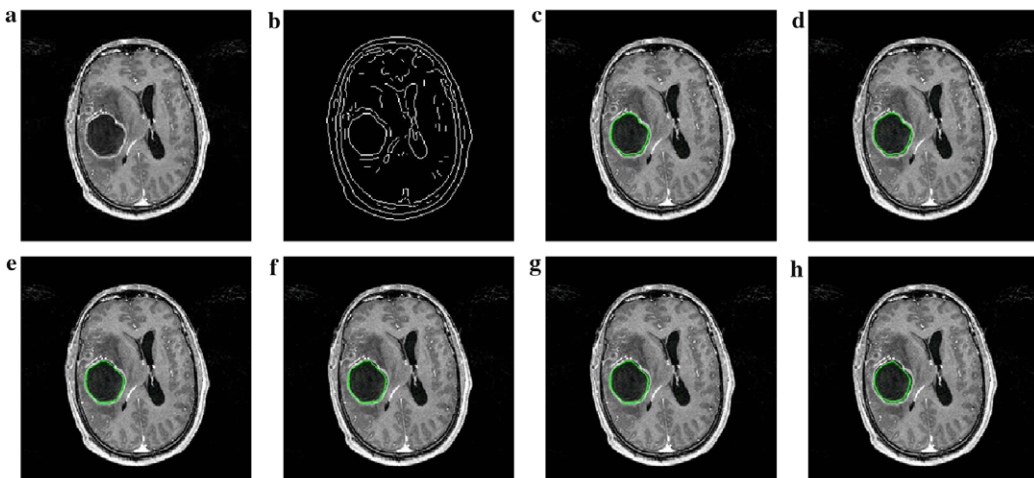


Fig. 18. Delineation of a resected tumor in an axial MR brain slice. (a) The axial slice. (b) The edges of the axial slice. (c)–(h) The segmentation results using R-snakes with the initial control points shown in Fig. 11 and standard deviations 0.015, 0.025, 0.035, 0.045, 0.055, and 0.065, respectively.

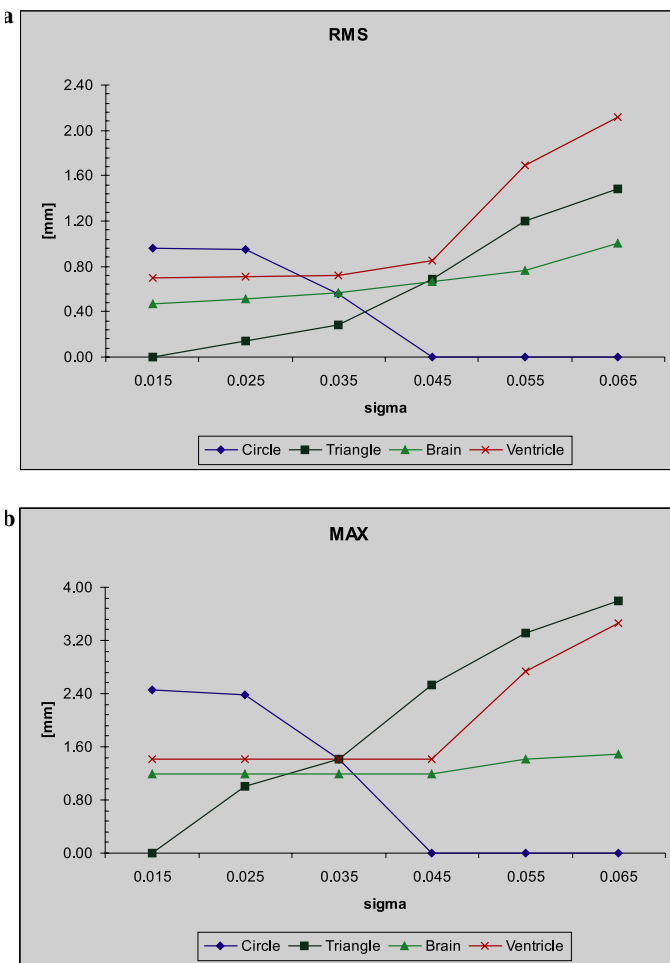


Fig. 19. (a) Root-mean-squared (RMS) and (b) maximum (MAX) segmentation errors in various experiments.

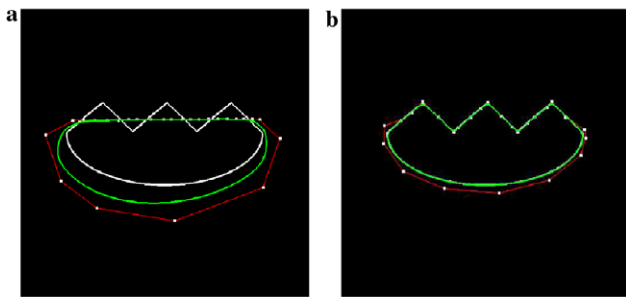


Fig. 20. Assigning different stiffnesses to different parts of a snake. (a) Initial position of the R-snake. (b) The shape recovered by the snake.

## 6.2. Varying local stiffness to minimize the control points

A property of the R-snake that is not shared by the B-snake is the ability to vary the smoothness along a recovered boundary. This property enables an R-snake to delineate a boundary that is partly smooth and partly detailed. An example of this is given in Fig. 20. The upper half of the shape in Fig. 20a contains sharp corners, while the lower half of the shape is very smooth. Letting the standard deviation at a node equal to the spacing between nodes at its sides, the snake shown in Fig. 20(b) is obtained.

When a snake defined by  $n$  control points is used and the stiffness of the snake is allowed to vary locally, spacing between the nodes is initially set equal to  $\sigma = 1/2n$ . Spacing between adjacent nodes is interactively changed, using image gradients at the points corresponding to the nodes. If by inserting two nodes to the sides of a given node, gradients at the new nodes remain high, it means that the newly added nodes are redundant and can be removed. Otherwise, they are kept. If by inserting two nodes to the sides of a node that has a low gradient the gradients at the new nodes remain low, it means that the snake is in a homogeneous area and the added nodes are redundant and can be removed. Otherwise, the newly added nodes are kept. This process is repeated until no more nodes can be added to the snake.

## 6.3. Coarse-to-fine segmentation

The presence of the stiffness parameters in R-snakes makes it possible to segment an image from coarse to fine. A snake with a small number of control points and a large standard deviation is initially used to find a coarse boundary of an object. The number of control points in the snake and the resolution of the image are gradually increased until the finest resolution image is segmented. At each intermediate resolution, since the initial position of the snake is close to its final position, a relatively small number of iterations is sufficient for the process to converge. At the coarsest resolution, since only a small number of control points is available and the correction step size is large, the process will converge quickly, resulting in an overall savings in computation time.

The coarse-to-fine segmentation process is demonstrated in Fig. 21. Fig. 21(a) shows initialization of an R-snake

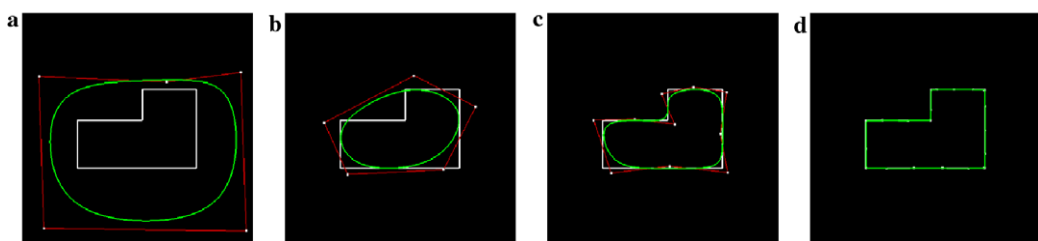


Fig. 21. The ability to dynamically vary the stiffness of the R-snake makes it possible to recover a shape from coarse to fine.

with five control points near a closed polygon, and Fig. 21(b) shows convergence of the snake to the polygon at the coarsest resolution. By gradually increasing the resolution of the image and decreasing the stiffness of the curve, the results shown in Fig. 21(c) and d are obtained. The number of iterations needed to get from (a) to (b), from (b) to (c), and from (c) to (d) were 65, 93, and 153, respectively.

The overhead in the coarse-to-fine approach involves the creation of an image pyramid that represents the image at different resolutions. This overhead can sometimes be larger than the time saved. If the object to be delineated is small or if a relatively good approximation to the boundary to be extracted is already known, the highest resolution image may be used from the start to find the desired boundary. However, if the boundary to be extracted is long and complex and the initial position of the snake is far from the final boundary, a coarse-to-fine approach should be used to find the boundary much quicker.

## 7. Summary and conclusions

A new representation for energy minimizing contours, called an R-snake, was introduced that is based on RaG curves. R-snakes have advantages over B-snakes. For instance, the stiffness along an R-snake can be varied to recover shapes containing smooth as well as detailed parts. The stiffness of an R-snake can be continuously varied to track a boundary from coarse to fine, enabling a higher speed at early stages of the process where the snake is distant from its final position.

Experimental results demonstrating segmentation of various synthetic and real images using R-snakes were presented. The main parameter to be determined in an R-snake is the number of control points  $n$ . The stiffness parameter of the snake is determined from the number of points:  $\sigma = 1/2n$ .  $n$  depends on the size and complexity of the shape to be recovered. Larger and more complex shapes require a larger number of control points to represent them. To reproduce more local details in a shape, a smaller  $\sigma$  should be used, while to smooth out noisy details in a shape, a larger  $\sigma$  should be used. If the complexity of the shape to be recovered is not known, a small number of control points can be initially selected to obtain a coarse approximation to the shape. The number of control points can then be increased as the stiffness of the snake is locally decreased to improve the localization accuracy of the delineated boundary.

## References

- [1] C. Kambhamettu, D.B. Goldgof, D. Terzopoulos, T. Huang, Nonrigid motion analysis, HPRIP-CV94 (1994) 405–430.
- [2] M. Kass, A. Witkin, D. Terzopoulos, Snakes: active contour models, Int. J. Comput. Vis. 1 (4) (1988) 321–331.
- [3] I. Choen, N. Ayache, P. Sulger, Tracking of points on deformable objects using curvature information, in: Proceeding of the European Conference on Computer Vision, 1992, pp. 459–466.
- [4] F. Leymarie, M. Levine, Tracking deformable objects in the plane using an active contour model, IEEE Trans. Pattern Anal. Machine Intelligence 15 (6) (1993) 635–646.
- [5] L.W. Chang, H.W. Chen, J.R. Ho, Reconstruction of 3D medical images: a nonlinear interpolation technique for reconstruction of 3D medical images, Comput. Vis. Graphics Image Process. 53 (4) (1991) 382–391.
- [6] L. Choen, On active contour models and balloons, CVGIP: Image Understanding 53 (2) (1991) 211–218.
- [7] L.D. Choen, I. Choen, Finite element methods for active contour models and balloons for 2D and 3D images, IEEE Trans. Pattern Anal. Machine Intelligence 15 (11) (1993) 1131–1147.
- [8] W.C. Lin, S.Y. Chen, A new surface interpolation technique for reconstructing 3d objects from serial cross-sections, Comput. Vis. Graphics Image Process. 48 (1989) 124–143.
- [9] A. Chakraborty, J.S. Duncan, Integration of boundary finding and region-based segmentation using game theory, Bizais (1995) 189–200.
- [10] J.M. Gauch, H.H. Pien, J. Shah, Hybrid boundary-based and region-based deformable models for biomedical image segmentation, Math. Meth. Med. Imaging III, SPIE Proc. 2299 (1994) 72–83.
- [11] C.S. Poon, M. Braun, R. Fahrig, A. Ginige, A. Dorrell, Segmentation of medical images using an active contour model incorporating region-based image features, Robb (1994) 90–97.
- [12] X. Chenyang, J.L. Prince, Snakes, shapes, and gradient vector flow, IEEE Trans. Image Processing 7 (3) (1998) 359–369.
- [13] D. Gil, P. Radeva, Curvature vector flow to assure convergent deformable models for shape modelling, Lect. Notes Comput. Sci. 2683 (2003) 261–274.
- [14] S. Menet, P. Saint-Marc, G. Medioni, B-snakes: implementation and application to stereo, in: Artificial Intelligence and Computer Vision. Proceedings of the Seventh Israeli Conference, 1990, pp. 323–326.
- [15] R. Cipolla, A. Blake, The dynamic analysis of apparent contours, in: Proceedings of the 3rd International Conference on Computer Vision, 1990, pp. 616–623.
- [16] D. Terzopoulos, H. Qin, Dynamic nurbs with geometric constraints for interactive sculpting, Acm. T. Graphic. 13 (2) (1994).
- [17] R. Meegama, J. Rajapakse, Nurbs snakes, Image Vis. Comput. 21 (2003) 551–562.
- [18] A. Goshtasby, Geometric modelling using rational Gaussian curves and surfaces, Computer Aided Design 27 (5) (1995) 363–375.
- [19] A.D. Aleksandrov, A.N. Kolmogorov, M.A. Lavrentev, Mathematics, Its Content, Methods, and Meaning, MIT Press, Cambridge, MA, 1964.
- [20] X.M. Pardo, P. Radeva, D. Cabello, Discriminant snakes for 3D reconstruction of anatomical organs, Med. Image Anal. 7 (2003) 293–310.
- [21] B. Levienaise-Obadia, A. Gee, Adaptive segmentation of ultrasound images, Image Vis. Comput. 17 (1999) 583–588.
- [22] C.W. Liao, G. Medioni, Simultaneous surface approximation and segmentation of complex objects, Comput. Vis. Image Understanding 73 (1) (1999) 43–63.
- [23] Y. Wang, E.K. Teoh, D. Shen, Structure-adaptive b-snake for segmenting complex objects, in: Proceedings of the 2001 International Conference on Image Processing, vol. 2, 2001, pp. 769–772.
- [24] Y. Wang, E.K. Teoh, D. Shen, A b-snake model using statistical and geometric information-applications to medical images, ICARV 2 (2002) 793–797.
- [25] Y. Wang, E.K. Teoh, D. Shen, Lane detection and tracking using b-snake, Image Vis. Comput. 22 (4) (2004) 269–280.
- [26] R. Cipolla, Active visual inference of surface shape, Lect. Notes Comput. Sci. 1016 (1995).